Lab on a Chip

View Online
Dynamic Article Links

Cite this: *Lab Chip*, 2011, **11**, 3873

www.rsc.org/loc

PAPER

Facile creation of hierarchical PDMS microstructures with extreme underwater superoleophobicity for anti-oil application in microfluidic channels†

Dong Wu,[a] Si-zhu Wu,[a] Qi-Dai Chen,[a] Shuai Zhao,[a] Hao Zhang,[a] Jian Jiao,[b] Jeffrey A. Piersol,[b] Jian-Nan Wang,[a] Hong-Bo Sun*[ac] and Lei Jiang*[d]

Received 14th March 2011, Accepted 23rd August 2011
DOI: 10.1039/c1lc20226j

Composition modification and surface microstructures have been widely utilized in interface science to improve the surface performance. In this paper, we observed a significant improvement of oil contact angle (CA) from 66 ± 2° to 120 ± 4° by introducing a radical silanol group on a flat PDMS surface through oxygen plasma pretreatment. By combining surface microstructures and plasma modification, we produced three kinds of superoleophobic surfaces: 20 μm pitch micropillar arrays, 2.5 μm pitch micropillar arrays and gecko foot-like hierarchical microstructures. Among them, the hierarchical surface with high surface roughness showed extreme underwater superoleophobicity, which featured ultrahigh CA (175 ± 3°) and ultrasmall sliding angle (<1°). Quantitative measurements demonstrated that these superoleophobic surfaces exhibited distinct adhesive behaviors, by which they were interpreted as Wenzel's, Cassie's and the Lotus state, respectively. A microfluidic channel with superoleophobic microstructures was further created by novel curve-assisted imprint lithography, and the characterization based on anti-oil contamination applications was carried out and discussed. We believe that the superoleophobic surfaces will power broad applications in oil microdroplet transportation, anti-oil channels and droplet microfluidic systems.

1. Introduction

Recently, with oil pollution becoming more and more serious, the design of self-cleaning anti-oil surfaces has been an urgent task because of broad potential applications from microfluidic devices[1] to household kitchenware and marine antifouling coatings.[2,3] For instance, integrated microfluidic devices[4a,b] exhibit many advantages, including small reagent requirements, short reaction time, portability, low cost, and low consumption of power; however, an open question when they deal with oil species in chemical analysis or cell culture applications is how to avoid cross contamination[4c] and increase the reusability of microfluidic devices. Likewise, in our daily life, bowls, scoops and clothes are often greased by all kinds of oil once they are contacted. Various detergents and organic solvents have been developed to clean them, but these chemical substances are not only potentially contaminative to living environments but also harmful to health after a long-term accumulation inside the human body. So, it is important to develop new methods and mechanisms to solve the problem of oil pollution. Fortunately, nature has given us inspiration to design functional surfaces.[5–15] Jiang *et al.* firstly found that fish could prevent their bodies from being stained by oil or plankton in the water.[16] Their investigation showed that the superhydrophilicity of a surface at the air/solid interface was crucial to its superoleophobicity (CA > 150°) at the water/solid interface. This offers a new avenue for preparing artificial anti-oil biomimetic surfaces. A variety of efforts[17–20] have been focused towards underwater superoleophobic surfaces by patterning hydrophilic materials. Although the oil CAs on these surfaces are greater than 150°, the most important function—the self-cleaning anti-oil ability enabling the oil on the surface to be removed by water—has not been reported.

In addition to surface microstructuring, choosing appropriate materials based on practical applications is important. The superoleophobic surfaces produced so far are subject to material limitations such as high cost (silicon[16]), poor biocompatibility (epoxy resin[17] and conducting polymer[18]) or instability (hydrogel[19,20]) to chemical solvents. So, it is indispensable to explore

[a]*State Key Laboratory on Integrated Optoelectronics, College of Electronic Science and Engineering, Jilin University, 2699 Qianjin Street, Changchun, 130023, China. E-mail: hbsun@jlu.edu.cn; jianglei@iccas.ac.cn*
[b]*Department of Electrical and Computer Engineering, University of Missouri–Columbia, Mo, 65211 Columbia, USA*
[c]*College of Physics, Jilin University, 119 Jiefang Road, Changchun, 130023, China*
[d]*Center of Molecular Sciences, Institute of Chemistry, Chinese Academy of Sciences, Beijing, China*
† Electronic supplementary information (ESI) available. See DOI: 10.1039/c1lc20226j

new materials to design underwater superoleophobic surfaces for a wide range of applications. As we know, PDMS is a type of economic, stable, and biocompatible material, which has been widely used in microfluidic devices[21a] for biological and chemical research. However, PDMS is a type of hydrophobic polymer with weak underwater oleophobic ability, which seriously limits its anti-oil applications. To the best of our knowledge, there are no reports about underwater superoleophobic PDMS surfaces. Moreover, integrating superoleophobic microstructures into microfluidic channels remains challenging due to the limitations of microfabrication technologies. The complex curved morphology of the microfluidic channel hindered the availability of microfabrication techniques such as ultraviolet photolithography, e beam, and X-ray lithography.

In this paper, we report gecko foot-like hierarchical microstructures made of PDMS, which were further treated with oxygen plasma etching.[21b,c] The treatment changed the flat PDMS surface from oleophilic (CA, 66 ± 2°) to oleophobic (120 ± 4°) by inducing a radical silanol group. The resulting hierarchical surfaces of high roughness exhibited extreme underwater superoleophobicity, with a CA greater than 170°, a sliding angle less than 1° and an adhesive force of about 1 μN, much more oleophobic than any single-level micropillar arrays. As a result, the contaminant droplet of seed oil on the gecko foot-like arrays was easily washed away by water, indicating that the artificial surface was promising as an effective self-cleaning anti-oil coating. Finally, a microfluidic channel with hierarchical microstructures was prepared by curve-assisted imprint lithography for anti-oil contamination application.

2. Experimental

Preparation of gecko foot-like microstructures

A frequency-tripled, Q-switched, single-mode Nd:YAG laser (Spectra-physics, American) with 355 nm wavelength was used for laser interference. A two-beam laser interference lithography system was set up as reported earlier.[22] Fig. 2(a) shows the fabrication scheme of the flexible superhydrophobic films. Firstly, the negative epoxy resin SU-8 2075 resin (Nano MicroChem Company, American) diluted with cyclopentanone (1:2 by volume) was spin-coated on a clean glass slide at 1000 rpm s^{-1} to achieve a 2.5 μm thickness. After being prebaked for 10 min at 95 °C to evaporate the organic solvent, the sample was exposed by two interference laser beams (diameter ≈ 9 mm and power ≈ 30 mW) to produce the grooved array structure with 2.5 μm pitch. The sample was rotated by 90° and irradiated for a second time. Then, it was further spin-coated with a 6 μm thickness SU-8 resin. After soft-baking, the 20 μm pitch grooves were fabricated on the sample by photolithography. The sample was baked for 10 min and developed in the SU-8 developer for 10 min. As shown in Fig. S2(a)†, a regular hole array template was obtained. The template was sealed with a layer of PDMS prepolymer. PDMS Sylgard 184 purchased from Dow Corning (MI) was chosen owing to its good elasticity, high optical transmission, and biocompatibility. The PDMS prepolymer cured in a conventional drying oven at 60 °C for 6 h. After being peeled off, the hierarchical PDMS pillar arrays were obtained [Fig. 2(d)].

Surface modification of PDMS samples

The PDMS samples were treated with oxygen plasma for 1 min (25 W) in a plasma reactor (790 Series, Plasma-Therm, Inc., Florida, USA) to activate the PDMS surface and increase its underwater oleophobicity.

The treatment time is about 2 minutes.

Sample characterization

The CA measurements were made by a Contact Angle System OCA 20 (Data Physics Instruments GmbH, Germany) at ambient temperature. The static CAs were measured by the sessile drop method with an oil droplet (4 μL). For detecting oils, 1,2-dichloroethane (DCE) was used. The morphologies of the regular SU-8 hole arrays and PDMS pillar arrays were characterized by a field emission scanning electron microscope (SEM, JSM-7500F, JEOL, Japan).

3. Results and discussion

Enhanced oleophobicity of flat PDMS surface by oxygen plasma treatment

From previous study,[16] we know that the superhydrophilicity of a surface in air is crucial for realizing superoleophobicity in water. However, PDMS shows high water CA [~115 ± 0.6°, Fig. 1(a)] in air due to its low-surface energy. When an oil droplet was placed on a flat PDMS surface in water, the CA under the three phase solid–water–oil contact interface was only 66 ± 2°

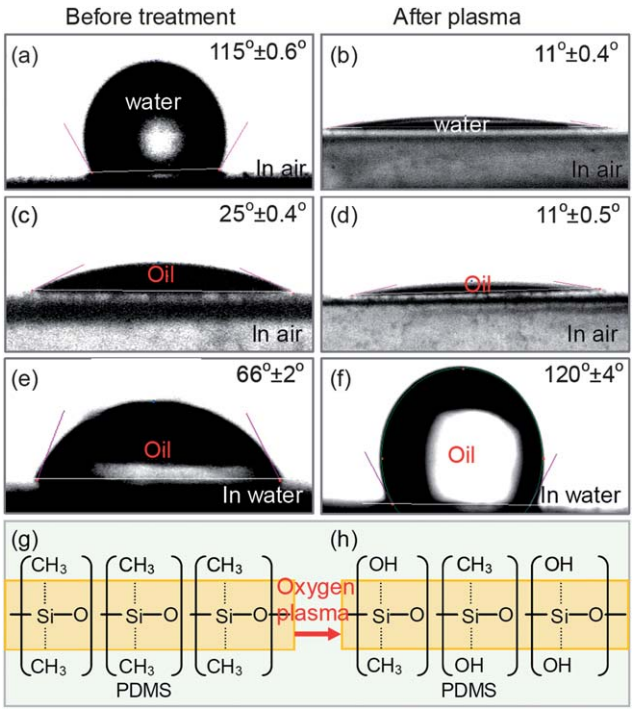

Fig. 1 Comparison of the wetting properties of the flat PDMS surface before and after oxygen plasma treatment. (a–f) Comparison of the water CAs in air, the oil CAs in air, and the oil CAs in water. After treatment, the oleophobicity dramatically increased (120 ± 4°). (g) and (h) are the chemical change of the PDMS surface by oxygen plasma treatment.

[Fig. 1(e)]. To increase its oil CA, a simple method, oxygen plasma etching, was used to activate the PDMS surface by inducing a radical silanol group.[23] The water CA was dramatically decreased to 11 ± 0.4° [Fig. 1(b)] and the oil CA varied from 25 ± 0.4° [Fig. 1(c)] to 11 ± 0.5° [Fig. 1(d)] in air. The CA of an oil droplet on the flat PDMS was significantly improved to 120 ± 4° [Fig. 1(f)] in water. To investigate the underlying mechanism, XPS spectra of the surfaces were measured [ESI, Fig. S1(a) and S1(b)†], which showed that the carbon peak intensity decreased significantly and the oxygen peak intensity increased after oxygen plasma treatment. The proportion of carbon was reduced from 47.9% to 36.8%, while the oxygen increased from 52.1% to 63.2%. The reason is that the original $-CH_3$ of the PDMS surface is converted into the hydrophilic group of OH, as shown in the schematic Fig. 1(g) and (h). This enhances the hydrophilicity and underwater oleophobicity of the PDMS surface. It is worth mentioning that the PDMS surface will become oleophilicity in air in about 3 hours as low molecular weight chains migrate to the surface to reduce the overall surface energy. The PDMS surface was therefore stored in water and was able to retain the oleophobicity for more than 20 days.

Preparation of hierarchical microstructures with extreme superoleophobic properties

The oxygen plasma treatment alone, although dramatically enhancing the oleophobicity of the PDMS surface, is still insufficient to realize superoleophobicity (CA > 150°), for which appropriate surface microstructures have to be further provided. Fig. 2(b) and (c) are 45° tilted view SEM images of 20 μm pitch and 2.5 μm pitch micropillar arrays realized by PDMS transfer of the hole template [ESI, Fig. S2(b) and (c)†] created by laser interference and photolithography. Both of the surfaces are superhydrophilic and superoleophilic in the air environment [the lower image of Fig. 2(b) and (c)], just as what we expected. In water, the oil CAs are 150 ± 2° and 164 ± 4° [Fig. 2(b) and 2(c)], indicating superoleophobicity. The superoleophobic surfaces were very stable when they were stored in water, as shown in the ESI, Fig. S3†. To further enhance the surface roughness, the above two types of pillar structures were combined together, producing gecko foot-like hierarchical microstructures [Fig. 2 (d)]. Around 16 small pillars stand on each big pillar, as calculated by the relative area of the rod top. The structures were repeatedly producible from templates [ESI, Fig. S2(a)†]. The measured oil CA reached as large as 175 ± 3°. The oil droplet easily rolled off from the sample surface, making CA measurement difficult. A small syringe was therefore used to fix the oil droplet. When the syringe was withdrawn, the oil droplet rolled down even if the sample surface was almost horizontal (titling angle < 1°) [Movie S1 and Fig. S4†]. This demonstrated that the gecko foot-like hierarchical arrays possessed extreme superoleophobicity.

Quantitative measurement of adhesive force between microstructures and oil droplet

In order to get deeper insight into the superoleophobic properties of microstructures, the adhesive force between oil and microstructures was systematically investigated. Although all these samples are underwater superoleophobic, they present distinct adhesive behaviors, as shown in Fig. 3(a). For the 20 μm pitch micropillar arrays and the flat PDMS surface, the oil droplet firmly stuck to the surface, implying high adhesive force. However, the oil droplet on 2.5 μm pitch pillar arrays exhibited

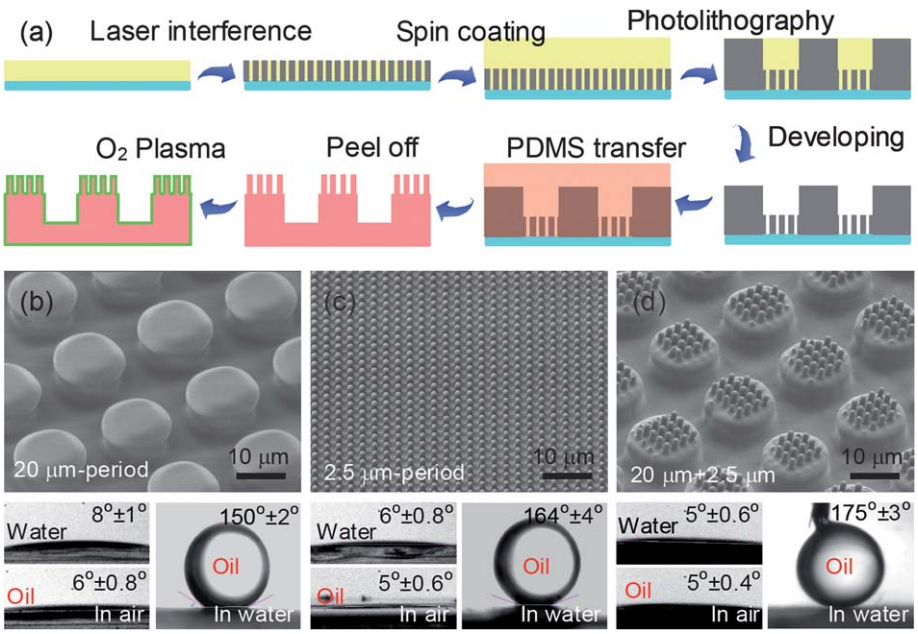

Fig. 2 (a) The fabrication scheme of gecko foot-like arrays. The main fabrication process: laser interference, photolithography, and PDMS transfer. (b)–(d) are 45° tilted SEM images of 20 μm period, 2.5 μm period pillar arrays, and hierarchical gecko foot-like microstructures. The insets in (b), (c) and (d) are the water and oil CA in air and underwater oil CA measurement, which revealed that the hierarchical microstructures showed extreme superoleophobic ability due to their high surface roughness.

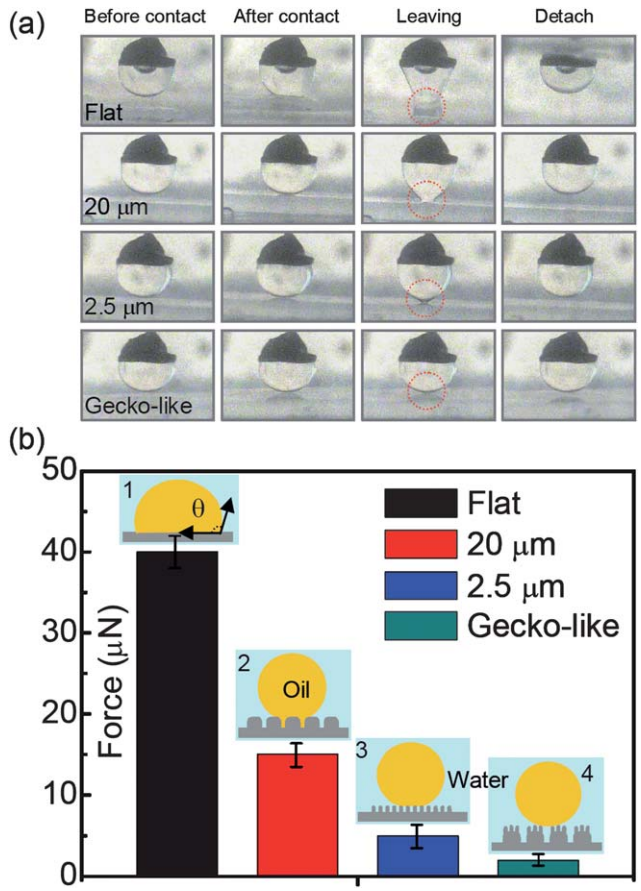

Fig. 3 (a) Dynamical adhesive force behaviors on different microstructures: flat PDMS surface, 20 μm period pillar arrays, 2.5 μm period pillar arrays, and hierarchical gecko foot-like arrays. (b) The adhesive forces for flat, 20 μm array, 2.5 μm array and gecko foot-like surface. The gecko foot-like microstructures showed the smallest adhesive force. The insets 1–4 are the schematic illustration of the underwater oil-adhesion mechanism on different surfaces. The flat PDMS surfaces and 20 μm period pillar arrays are in Wenzel's state. The 2.5 μm period pillar arrays are in Cassie's state while the hierarchical gecko foot-like microstructures are in the Lotus state.

low adhesive force, and the force from the gecko foot-like arrays was even smaller. For quantitative measurement, a high-sensitivity micromechanical balance system[22] was used [Fig. 3(b)]. The force–distance curves for different surfaces are shown in the ESI, Fig. S5†. The adhesive force on the 20 μm period micropillar arrays surface is about 15 μN while the one on the flat PDMS surface is larger than 40 μN. In contrast, the adhesive force significantly decreases to 5 μN on the 2.5 μm period micropillar array surface, and the one on the gecko foot-like arrays is too small to measure (detection limit is 1 μN).

The underlying physical mechanism of different superoleophobicity surfaces

According to the above experimental result, we know that the flat surface and 20 μm period pillar arrays exhibit high adhesive force and lower oil CA. This means that the surface is in Wenzel's superoleophobic state [the inset 1 and 2 of Fig. 3(b)]. The strong adhesion between the oil and PDMS pillars was mainly caused by van der Waals' forces. The bigger the contact area, the stronger the adhesive force. In air, the wettability of the solid surface was widely characterized by the contact angle along Young's equation,[13b] which was also applicable to a liquid droplet on a liquid/solid surface.[24] The contact angle was calculated according to Wenzel's formula,[25]

$$\cos\theta_w = k\cos\theta_y$$

where θ_w is the apparent CA on a rough surface and θ_y is the ideal CA (Young's angle) of an oil droplet on a smooth surface in the water environment. The roughness factor $k = (1 + 2R\pi h/d_1^2)$ is defined as the ratio of the actual surface area over the projected area.[26] Given $R = 7.5$ μm, $h = 6$ μm and $d_1 = 20$ μm, we have $k = 1.71$ and $\theta_w = 148°$, agreeing with the measured value $150 \pm 2°$.

The 2.5 μm period pillar arrays showed lower adhesive force and bigger CA, meaning that the surface was in a composite underwater superoleophobic state [the inset 3 of Fig. 3(b)]. In this state, the oil droplet sat on the pillar arrays, and water was trapped below the oil droplet. According to Cassie's formula,

$$\cos\theta_w = f\cos\theta_y + f - 1$$

where f is the area fraction of the projected wet area. Here $f = \pi R^2/d_2^2$, where R is the tip radius of the pillar and d_2 is the center-to-center pitch. The smaller the solid fraction, the better the oleophobic ability. Given $R = 0.5$ μm and $d_2 = 2.5$ μm, we can get $f = 0.126$, and the oil CA $\theta_w = 160°$. The hierarchical microstructures could significantly reduce the contact area between the oil droplet and the PDMS microstructures. Therefore, the surface showed ultralow adhesive force and smaller oil CA hysteresis, indicating the surface was in the "Lotus" state [Fig. 3(f)], a special case of Cassie's state. The calculated value $f = 16 \times \pi R^2/d_1^2$ is about 0.0314, so the oil CA is about 170°, agreeing well with the measured value.

Self-cleaning anti-oil ability of microstructured surfaces

Due to the ultralow adhesive force of oil in water, the gecko foot-like microstructure surface could be considered as a kind of self-cleaning anti-oil layer for practical applications. As shown in Fig. 4(a), a droplet of soybean oil [ESI, Table S1†], the most common oil used in foods, was dropped onto the surface [image 1]. When the surface was immersed into water [image 2], the oil was removed by the water without any residues [image 3]. In our experiment, the self-cleaning anti-oil process was investigated by *in situ* optical microscopy, as shown in Fig. 4(b) and Movie S2†. To clearly observe the anti-oil effect, the experimental process was also monitored from the perpendicular direction [Fig. 4(c) and Movie S3†]. For comparison, we found that the flat region of the sample did not exhibit the anti-oil ability. The oil on the flat region could not be washed away, as shown in Fig. 4(c)-3. Moreover, the oil on the hierarchical microstructures without plasma treatment firmly adhered to the surface and could not be washed away [Fig. S6 and Movie S4†], implying that both the surface microstructures and plasma treatment were crucial to the self-cleaning anti-oil ability.

Although both the underwater superoleophobic anti-oil surface and the superhydrophobic (in air) anti-dust surface

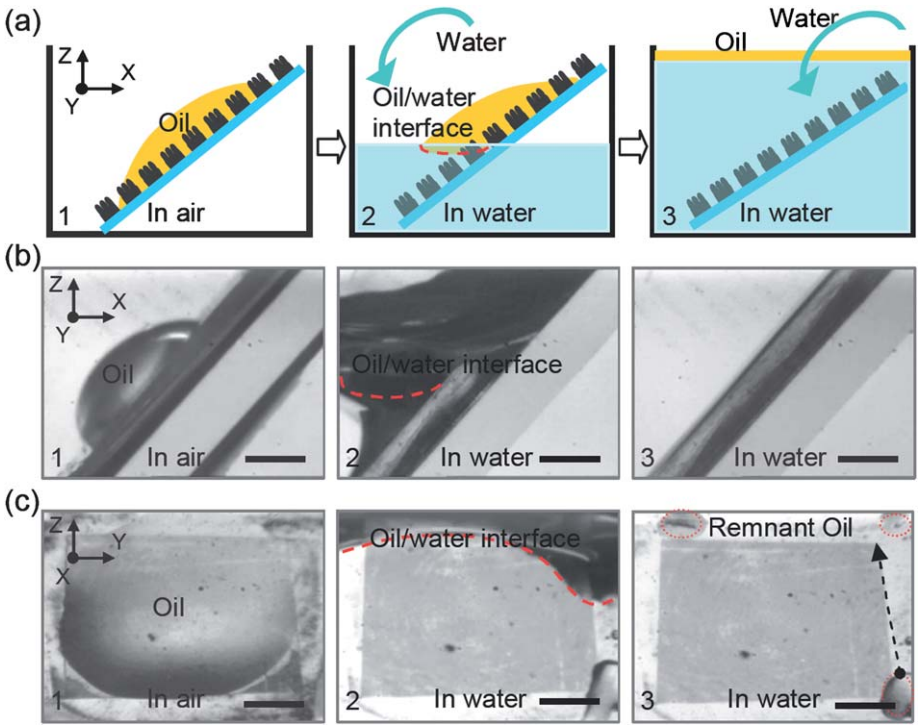

Fig. 4 (a) Schematic illustration of self-cleaning anti-oil ability of extreme superoleophobic surfaces. The experimental process consists of three steps. A seed oil droplet was dropped on the superoleophobic microstructure surface [image 1]. Then, water was added and the oil was gradually removed by the water [image 2]. Finally, the oil on the microstructured surface was washed out by water [image 3]. (b) A series of microscopic images of the experimental results obtained by *in situ* optical microscopy. (c) The same experiment which was observed from the perpendicular direction. We could find that the oil on the microstructure region was removed. However, there was remnant oil on the flat region [the red round region of image 3]. The scale bar is 1 mm.

exhibited self-cleaning effect, they may originate from distinct physical mechanisms. As we know, the self-cleaning superhydrophobic surface showed high CA and low SA. After putting a water droplet on the surface, the dust particles adhered to the water and were removed during the water rolling process [Fig. S7 (a)†]. However, the self-cleaning anti-oil surface was superhydrophilic. It was believed that the oil was removed by the water injection. There were possibly two main forces to push out the oil from the surface. The first one is the surface tension of oil/water/air interface F_s. The second one is the hydrophilic force F_h due to the superhydrophilicity of the surface. The more the hydrophilicity of one surface, the stronger the hydrophilic force. Once the water was added, the oil was removed by both of the forces, as shown in the schematic image Fig. S7(b)†. Although the first force also existed on the flat surface, it could not remove the oil due to the weak hydrophilic force. Therefore, the second force determined by the surface microstructures was crucial to anti-oil function.

Microfluidic channel with hierarchical microstructures prepared by curve-assisted imprint lithography

Due to their anti-oil ability, the hierarchical microstructures were integrated into a microfluidic channel for free-contamination application. Here, we developed a new method, which we named curve-assisted PDMS imprint lithography [Fig. 5(a)], to prepare the microfluidic channel with hierarchical microstructures [Fig. 5 (b)]. First, after being modified by a fluoroalkylsilane ($CF_3(CF_2)_5CH_2CH_2SiCl_3$) through thermal chemical vapor deposition for 2 h at 60 °C as an anti-stick layer, the hierarchical microstructures [Fig. 2(e)] were transferred into the PDMS hole template. Due to the inherent flexibility of PDMS, the template was curved and further transferred by PDMS. Then, the microfluidic channel with microstructures [Fig. 5(b)] was formed and sealed by PDMS hierarchical microstructures. The radius of the curved microfluidic channel is about 800 μm, which is determined by the thickness (~300 μm) of the flexible PDMS films and the radius (500 μm) of the curved column. The dimension of the anti-oil microfluidic channel may be reduced to the order of 100 μm if a thin-film with a 100 μm thickness and a 50 μm radius copper thread was used. For comparison, the flat channel [Fig. 5 (c)] was prepared and its anti-oil ability was investigated [Fig. 6 (a)]. At the flat region, the oil could not be washed away by water because the oil firmly adhered to the channel [Fig. 6(b) and Movie S5†] while no oil existed on the microstructure region [Fig. 6(c) and Movie S6†]. Furthermore, the channel was opened and carefully observed by optical microscopy. There was remnant oil on the flat region [Fig. 6(b)-3] while no oil existed on the microstructured region [Fig. 6(c)-6].

Conclusion

In conclusion, a simple strategy, oxygen plasma, was proposed to enhance the oleophobicity (120 ± 4°) of a PDMS surface by inducing a radical silanol group. Superoleophobic PDMS biosurfaces were prepared by combining photolithography, soft

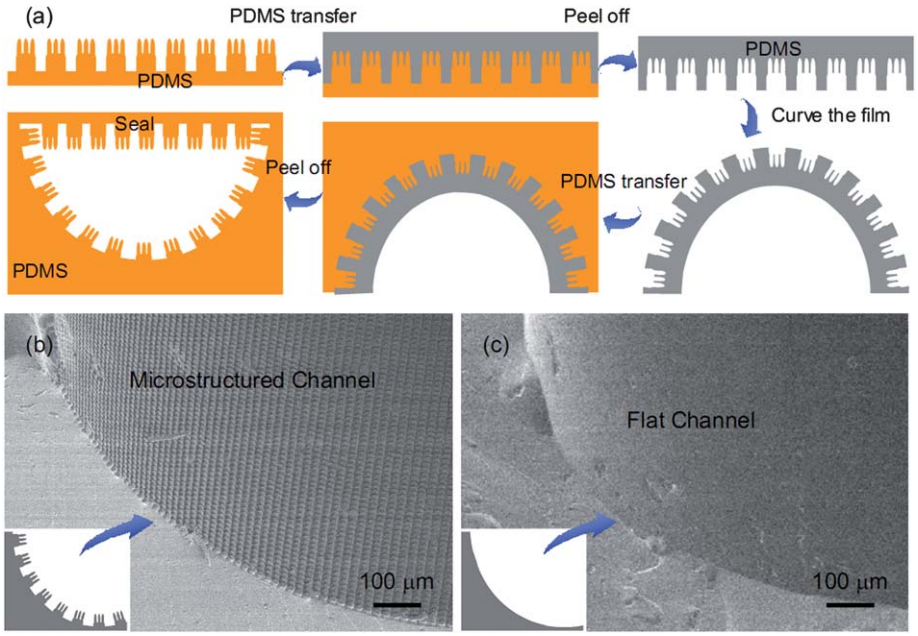

Fig. 5 Self-cleaning anti-oil application in the microfluidic channel. (a) Schematic illustration of the fabrication process of microstructured channel—curve-assisted PDMS imprint lithography. (b) SEM image of microfluidic channel with hierarchical microstructures. (c) SEM image of flat microfluidic channel.

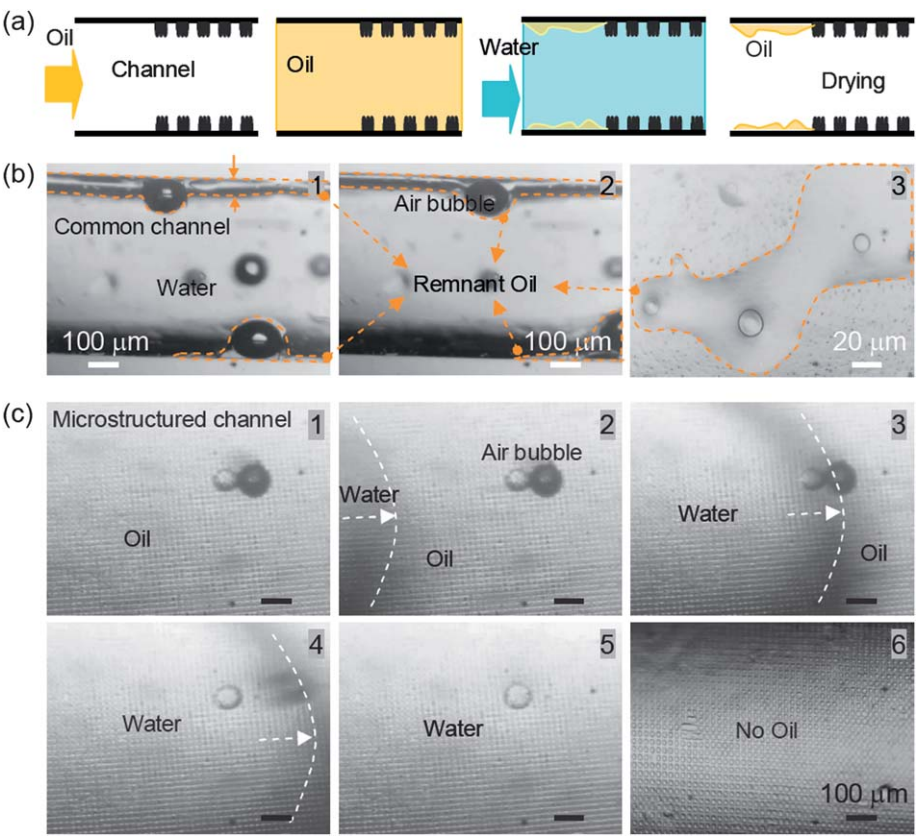

Fig. 6 Comparison of a flat channel and microstructured channels. (a) Schematic illustration of the experimental process. Firstly, the oil was imported into the channel. Then, the water was used to clean the channel. Finally, the flat region and microstructured region were dried. (b) The oil droplet on the flat microfluidic channel. The oil firmly adhered to the channel and could not be washed out by water. (c) The self-cleaning anti-oil ability of the microfluidic channel with hierarchical microstructures. We could find that the oil on the flat region could not be removed while there is no oil on the microstructured channel. The air bubble was put into the microfluidic channels to better observe the self-cleaning oil function.

lithography, and oxygen plasma modification. Their oleophobic properties and underlying physical mechanisms were systematically investigated. It was found that the oil droplet on the hierarchical surface could be easily washed away by water, which showed the superoleophobic surface could be considered as a kind of effective anti-oil coating. Moreover, we developed curve-assisted imprint lithography to realize a microfluidic channel with hierarchical microstructures for anti-oil contamination. We believe that the gecko foot-like array surfaces which are readily batch produced by soft lithography of the template will find broad applications in oil-repellent ship coatings, anti-oil textiles and lab-on-a-chip systems.[27]

Acknowledgements

This work was supported by 973 Program (Grant #2011CB013005) and NSFC (Grant #60978048, 61008035 and 90923037).

References

1 L. Ionov, N. Houbenov, A. Sidorenko, M. Stamm and S. Minko, *Adv. Funct. Mater.*, 2006, **16**, 1153.
2 B. A. Starkweather, X. G. Zhang and R. M. Counce, *Ind. Eng. Chem. Res.*, 2000, **39**, 362.
3 R. Sheparovych, M. Motornov and S. Minko, *Adv. Mater.*, 2009, **21**, 1840.
4 (*a*) S. Zeng, B. Li, X. Su, J. Qin and B. Lin, *Lab Chip*, 2009, **9**, 1340; (*b*) W. Zheng, Z. Wang, W. Zhang and X. Y. Jiang, *Lab Chip*, 2010, **10**, 2906; (*c*) K. D. Dorfman, M. Chabert, J. H. Codarbox, G. Rousseau, P. D. Cremoux and J. L. Viovy, *Anal. Chem.*, 2005, **77**, 3700.
5 C. Neinhuis and W. Barthlott, *Ann. Bot.*, 1997, **79**, 667.
6 X. F. Gao and L. Jiang, *Nature*, 2004, **432**, 7013.
7 (*a*) X. Yu, Z. Q. Wang, Y. G. Jiang, F. Shi and X. Zhang, *Adv. Mater.*, 2005, **17**, 1289; (*b*) C. Greiner, E. Arzt and A. Del Campo, *Adv. Mater.*, 2009, **21**, 479; (*c*) S. Z. Wu, J. N. Wang, L. G. Niu, J. Yao, D. Wu and A. W. Li, *Appl. Phys. Lett.*, 2011, **98**, 081902.
8 (*a*) Y. H. Xiu, L. B. Zhu, D. W. Hess and C. P. Wong, *Nano Lett.*, 2007, **7**, 3388; (*b*) W. L. Min, B. Jiang and P. Jiang, *Adv. Mater.*, 2008, **20**, 3914.
9 (*a*) J. Hong, W. K. Bae, H. Lee, S. Oh, K. Char, F. Caruso and J. Cho, *Adv. Mater.*, 2007, **19**, 4364; (*b*) I. A. Larmour, G. C. Saunders and S. E. J. Bell, *Angew. Chem., Int. Ed.*, 2008, **47**, 5043.
10 (*a*) L. Zhai, F. C. Cebeci, R. E. Cohen and M. F. Rubner, *Nano Lett.*, 2004, **4**, 1349; (*b*) L. J. Ci, S. M. Manikoth, X. S. Li, R. Vajtai and P. M. Ajayan, *Adv. Mater.*, 2007, **19**, 3300.
11 (*a*) S. Srinivasan, V. K. Praveen, R. Philip and A. Ajayaghosh, *Angew. Chem., Int. Ed.*, 2008, **47**, 5750; (*b*) Z. Z. Luo, Z. Z. Zhang, L. T. Hu, W. M. Liu, Z. G. Guo, H. J. Zhang and W. J. Wang, *Adv. Mater.*, 2008, **20**, 970; (*c*) D. Wu, Q. D. Chen, H. Xia, J. Jiao, B. B. Xu, X. F. Lin, Y. Xu and H. B. Sun, *Soft Matter*, 2010, **6**, 263; (*d*) D. Wu, J. N. Wang, S. Z. Wu, Q. D. Chen, S. Zhao, H. Zhang, H. B. Sun and L. Jiang, *Adv. Funct. Mater.*, 2011, **21**, 2927.
12 (*a*) Z. Z. Gu, H. Uetsuka, K. Takahashi, R. Nakajima, H. Onishi, A. Fujishima and O. Sato, *Angew. Chem., Int.Ed.*, 2003, **42**, 894; (*b*) V. Jokinen, L. Sainiemi and S. Franssila, *Adv. Mater.*, 2008, **20**, 3453.
13 (*a*) P. Gould, *Mater. Today*, 2003, **6**, 44; (*b*) A. Nakajima, K. Hashimoto and T. Watanabe, *Monatsh. Chem.*, 2001, **132**, 31.
14 A. Lafuma and D. Quéré, *Nat. Mater.*, 2003, **2**, 457.
15 (*a*) B. Zhao, J. S. Moore and D. J. Beebe, *Science*, 2001, **291**, 1023; (*b*) B. Bhushan, K. Koch and Y. C. Jung, *Soft Matter*, 2008, **4**, 1799.
16 M. J. Liu, S. Wang, Z. Wei, Y. Song and L. Jiang, *Adv. Mater.*, 2009, **21**, 665.
17 Y. C. Jung and B. Bhushan, *Langmuir*, 2009, **25**, 14165.
18 M. Liu, F. Q. Nie, Z. Wei, Y. Song and L. Jiang, *Langmuir*, 2009, **26**, 3993.
19 L. Chen, M. Liu, L. Lin, T. Zhang, J. Ma, Y. Song and L. Jiang, *Soft Matter*, 2010, **6**, 2708.
20 L. Lin, M. Liu, L. Chen, P. Chen, J. Ma, D. Han and L. Jiang, *Adv. Mater.*, 2010, **22**, 4826.
21 (*a*) J. C. Mcdonald and G. M. Whitesides, *Acc. Chem. Res.*, 2002, **35**, 491; (*b*) M. Morra, E. Occhiello, R. Marola, F. Garbassi, P. Humphrey and D. Johnson, *J. Colloid Interface Sci.*, 1990, **137**, 11; (*c*) J. Zhou, A. V. Ellis and N. H. Voelcker, *Electrophoresis*, 2010, **31**, 2.
22 (*a*) D. Wu, Q. D. Chen, J. Yao, Y. C. Guan, J. N. Wang, L. G. Niu, H. H. Fang and H. B. Sun, *Appl. Phys. Lett.*, 2010, **96**, 053704; (*b*) D. Wu, S. Z. Wu, Q. D. Chen, Y. L. Zhang, J. Yao, X. Yao, L. G. Niu, J. N. Wang, L. Jiang and H. B. Sun, *Adv. Mater.*, 2011, **23**, 545; (*c*) D. Wu, Q. D. Chen, B. B. Xu, J. Jiao, Y. Xu, H. Xia and H. B. Sun, *Appl. Phys. Lett.*, 2009, **95**, 091902; (*d*) D. Wu, Y. B. Zhao, S. Z. Wu, Y. F. Liu, H. Zhang, S. Zhao, J. Feng, Q. D. Chen, D. G. Ma and H. B. Sun, *Opt. Lett.*, 2011, **36**, 2635.
23 S. H. Tan, N. T. Nguyen, Y. C. Chua and T. G. Kang, *Biomicrofluidics*, 2010, **4**, 032204.
24 M. Järn, B. Granqvist, J. Lindfors, T. Kallio and J. B. Rosenholm, *Adv. Colloid Interface Sci.*, 2006, **123**, 137.
25 R. N. Wenzel, *Ind. Eng. Chem.*, 1936, **28**, 988.
26 Z. Yoshimitsu, A. Nakajima, T. Watanabe and K. Hashimoto, *Langmuir*, 2002, **18**, 5818.
27 D. Wu, Q. D. Chen, L. G. Niu, J. N. Wang, R. Wang, H. Xia and H. B. Sun, *Lab Chip*, 2009, **9**, 2391.